Smart Host Microcontroller for Optimal Battery Charging in a Solar-Powered Robotic Vehicle

Tomás de J. Mateo Sanguino and Justo E. González Ramos

***Abstract*—This paper focuses on the design and construction of an optimization charging system for Li–Po batteries by means of tracked solar panels. Thus, the implementation of a complete energy management system applied to a robotic exploration vehicle is put forward. The proposed system was tested on the VANTER robotic platform—an autonomous unmanned exploration vehicle specialized in recognition. The interest of this robotic system lies in the design concept, based on a smart host microcontroller. On this basis, our proposal makes a twofold significant contribution. On the one hand, it presents the construction of a solar tracking mechanism aimed at increasing the rover's power regardless of its mobility. On the other hand, it proposes an alternative design of power system performance based on a pack of two batteries. The aim is completing the process of charging a battery independently while the other battery provides all the energy consumed by the robotic vehicle.**

***Index Terms*—Li–Po battery, mechatronic system, photovoltaic (PV), robotic vehicle, solar tracker.**

Nomenclature

C_1	Capacitor in parallel between PV system and charger.
$I_{\rm ch}$	Current at the charger input.
I_L	Current through the load system.
$I_{\rm MPP}$	Current of the PV panel at the maximum power point.
$I_{\rm sc}$	Short circuit current.
n	Number of panels in the PV system.
$P_{\rm bat}$	Power consumed by the battery during charging.
$P_{\rm max}$	Maximum power of a PV panel.
P_s	Power supplied by a PV panel.
$P_{\rm schottky}$	Power consumed by the protection diode of a PV panel.
$R_{\rm int}$	Internal resistor of a battery.
R_L	Test resistor for battery charging and discharging.
t	Time for battery charging and discharging.
$t_{\rm on}$	Backup time for a battery.
$t_{\rm trans}$	Time for the battery switching.
$V_{\rm ch}$	Voltage at the charger input.
$V_{\rm cutoff}$	Cutoff voltage for the battery discharging.
$V_{\rm cv}$	Battery cells voltage.
$V_{\rm end}$	Maximum voltage for the battery discharging.
$V_{\rm int}$	Voltage drop across $R_{\rm int}$.
$V_{\rm MPP}$	Voltage of the PV panel at the maximum power point.
$V_{\rm oc}$	Open circuit voltage.
V_s	Supply voltage of the PV system.
$V_{\rm up}$	Protection condition voltage for battery charging.
x	Lighting difference between each pair of photosensors.

Manuscript received January 16, 2012; accepted April 5, 2012. Date of publication May 10, 2012; date of current version January 18, 2013. Recommended by Technical Editor G. Herrmann. This work was supported in part by the research group TEP-192 "Control and Robotics" and in part by teaching innovation projects at the University of Huelva, Huelva, Spain.

T. de Jesus Mateo Sanguino is with the Department of Ingeniería Electrónica, Sistemas Informáticos y Automática, University of Huelva (ETSI La Rábida), Huelva 21071, Spain (e-mail: tomas.mateo@diesia.uhu.es).

J. E. González Ramos is with Abengoa Solar, 41014 Seville, Spain (e-mail: etogonza@gmail.com).

Color versions of one or more of the figures in this paper are available online at http://ieeexplore.ieee.org.

Digital Object Identifier 10.1109/TMECH.2012.2195499

I. Introduction

SOLAR power systems in autonomous robotic vehicles have been often used for some years. A real example is the Sojourner rover, in which most of the supplied energy is generated by a reduced-size photovoltaic (PV) panel [1]. However, in case of scarce to no solar light, the rover should minimize consumption, since its batteries in line could not be recharged when depleted [2]. The use of rechargeable batteries in a space mission was used for the first time in the Mars Exploration Rovers. Nevertheless, the need for greater operation autonomy by Spirit and Opportunity was solved by means of larger deploy solar panels [3]. This solution works as the basis for the design of solar panels for the future ExoMars mission. This rover, thanks to its high-efficiency ultrathin-film silicon cells constructed on carbon-fiber reinforced plastic, is capable of providing higher power [4], [5]. NASA designs inspired different generations of exploration vehicles [6]. This is the example of K9, a rover for remote science exploration and autonomous operation [7]; field integrated design and operations, an advanced-technology prototype by Jet Propulsion Laboratory for long-range mobile planetary science [8]; and Micro5, a series of robotic vehicles devised for lunar exploration [9]. As its main design advantage, this rover series has a dual solar panel system coupled to an assisted suspension mechanism. This prevents the manipulator arm mounted on the middle of the rover from having to minimize solar panel-generated power and allows it to dust solar panel surface.

Other robotic exploration vehicles have also been developed in academic spheres. This is the case of SOLERO, developed by the École Polytechnique Fédérale de Lausanne, which reached optimal energy consumption by a combination of a smart power management and an efficient locomotion system [10], [11]. On the other hand, the Carnegie Mellon University developed Hyperion, a rover in which the major technological milestone was

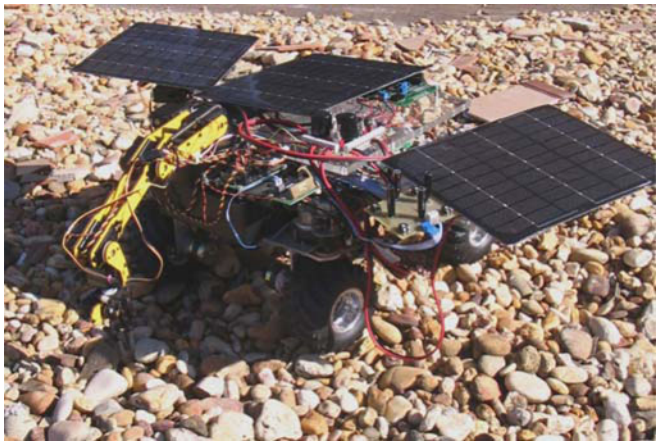

Fig. 1. VANTER: a solar-powered robotic vehicle.

the implementation of solar-synchronous techniques to increase the amount of energy generated by solar panels [12]; and Zoë, a rover capable of long-distance traverses under extreme environmental conditions devoted to science investigation at the Atacama desert [13]. With an educational approach, Carnegie Mellon University also developed a personal exploration vehicle called PER [14]. More recently, Lever and coworkers [15] and [16] have described the concepts of modeling, design, and fabrication of a robot-box prototype to be used in polar environments. The platform—known as Cool Robot—uses a control algorithm of maximum power point (MPP) aimed at maximizing system-supplied power for five PV modules designed as a cube. Finally, there are some noteworthy projects which main achievement is the optimal selection of solar energy and different power sources according to the operation conditions of a robot [17]–[19].

The VANTER robotic exploration vehicle aims to improve various aspects of the aforementioned rovers with scientific and academic purposes. To introduce the developed robot (see Fig. 1), the main features and properties are compared in Table I. Subsequently, this paper is organized as follows. The next section presents the mobile robotic system. Its main features are described and its hardware and software architecture are presented. Section III introduces the concept of smart host microcontroller (SHM) for intelligent power management applied to an exploration vehicle. The following sections present the control of the battery-charging system by means of tracked solar panels, which is the main aim of this paper; the design of its mechanical structure, its electronic devices and the graphical user interface (GUI) are presented. Section IV aims at providing the necessary parameters for the batteries sizing, charging, and discharging algorithm, and the PV system sizing. Therefore, Section V puts into practice the developed methodology by testing the rover power systems. Finally, the results and findings from the developed work are presented.

II. Mobile Robotic Platform

VANTER—Spanish acronym for autonomous unmanned exploration vehicle specialized in recognition—is a robotic exploration vehicle developed at the University of Huelva, Huelva, Spain [20]. The rover was developed to be guided and has a set of four wheels coupled to a plane chassis that can rotate independently. The four-wheel-drive (4WD) and the individual control of each wheel allow different types of movement; including Ackerman configuration, the crabbing maneuver or the rotation with inner inertial center. The four wheels in VANTER are sustained by means of independent passive suspension of double aluminum fork to absorb terrain vibrations. Each wheel consists of two motors, one for rotation and another for driving. On the one hand, forward movement is produced by means of dc motors (12 V and 60 mA) that provides 120 r/min with a torque of 8.87 kg/cm. On the other hand, the rotation motor provides a speed of 152 r/min Among others instruments aboard VANTER disposes of a 5-DOF robotic arm, an OmniVision MC203 wireless microcamera, and an analog video receiver with a Pinnacle Dazzle DVC100 video capture card [20]. Its reduced weight, small dimensions, and versatility make VANTER suitable as a robotic exploration vehicle (see Table I).

The robotic system programming is divided into three main code levels and its hardware was designed with a hierarchical control structure based on modular microcontrollers (see Fig. 2). The top level program, carried out in LabVIEW language, is executed in a remote PC and offers a GUI to monitor and control the whole robotic vehicle [21]. The second code level, programmed in C language, runs autonomously on a master PIC16F876A microcontroller aboard VANTER. Communication with the remote PC is performed by using a UHF modem for the centralized control of rover functions. The third code level consists of several slave microcontrollers distributed in an I^2C network aimed at the distributed control of the VANTER driving functions ($4 \times$ PIC16F88), remote manipulation, and power management.

III. Mechatronic System Design

A typical power management design consists of smart batteries integrating both communication devices and electronics able to control the charge. However, when an economical system is required, the concept of intelligence should be applied to software design for simple batteries. One of the main objectives of this paper is the implementation of the SHM concept to develop a low-cost power management system aboard a robotic vehicle. The system consists of an electrical circuit interconnecting a PV system, a charger device, a selector system, a batteries monitor system, and a battery system (see Fig. 3).

The SHM is based on a PIC16F886 microcontroller, which monitors VANTER consumption and decisions in a completely autonomous way [22]. The SHM has two main functions: 1) detecting environmental light level and controlling the solar tracking system to obtain the highest power; and 2) interpreting operation data from batteries and solar panels to control the working mode of the charger accordingly. The cost of this system—regardless of the navigation instruments and VANTER software—is US$ 600.

TABLE I
DESIGN FEATURES OF SOME ROVERS WITH SCIENTIFIC AND ACADEMIC GOALS

Name	CPU	Battery System	Solar Panel	Size & Weight	Wheels	Speed	Year
Sojourner	1 x 80C85 Processor	3 x $LiSoC_{12}$ (12.4 kg/u, 150 Wh)	1 x 18 GaAs/Ge cells (0.22 m^2, 18.2 %, 15.3 W)	0.65 x 0.48 x 0.3 m^3, 11Kg	6	1 cm/s	1.997
Micro5 Series	1 x RISC Processor	NiCd & Lithium	2 x 27 W to 40 W	0.53 x 0.55 x 0.25 m^3, 5 Kg to 30 Kg	5	1.5 cm/s	2.001
Hyperion	CompactPCI Pentium III	2 x acid gel-cells (150 W)	2 x Si cells (3.45 m^2, 12.8%, 440 W)	2 x 2.4 x 3 m^3, 157 Kg	4	0.3 m/s	2.001
SOLERO	1 x Laptop & 1 x Microcomputer	2 x NI-Mh (700 mA, 8W)	1 x 10LiTHI-ETA® (0.3m^2, 17 %, 14 W)	0.88 x 0.6 x 0.45 m^3, 12 Kg	6	0.5 m/s	2.002
MER	1 x RAD6000 PowerPC	2 x Li-Ion (7.15 Kg/u, 600 Wh)	GaInP/GaAs/Ge cells (1.2 m^2, 23.8%, 100W)	2.3 x 1.6 x 1.5 m^3, 174 Kg	6	5 cm/s	2.003
Zoë	2 x Pentium IV, 1 x Pentium III & 1 x AMD SC520	2 x Li-Po (1500 Wh)	1 x GaAs cells (23 %, 2.4 m^2)	1.63 x 2 m^2, 198 Kg	4	0.9 m/s	2.005
PER	1 x PIC Microprocessor & 1 x ARM Processor	4 x NiMh (86.4 Wh)	_	0.36 x 0.33 x 0.24 m^3, 6.8 Kg	6	4 cm/s	2.006
Cool Robot	1 x 8-bits Microcontroller	3 x Li-Ion (12 Ah, 520 Wh)	5 x A-300 Sunpower® (7.2 m^2, 18.4 %, 270 W)	1.4 x 1.5 x 1 m^3, 80 Kg	4	0.4 m/s	2.006
VANTER	6 x 8-bits Microcontrollers	2 x Li-Po (0.15 Kg/u, 2400 mAh)	3 x PET (0.15 m^2, 12 %, 18 W)	0.35 x 0.75 x 0.3 m^3, 12 Kg	4	0.6 m/s	2.010
ExoMars	2 x LEON Processors & 1 x FPGA Co-processor	2 x Li-Ion (9.25 Kg/u, 1250 Wh)	5 x GaAs cells (1.45 m^2, 19%, 120W)	150 Kg to 205 Kg	6	1 cm/s	_

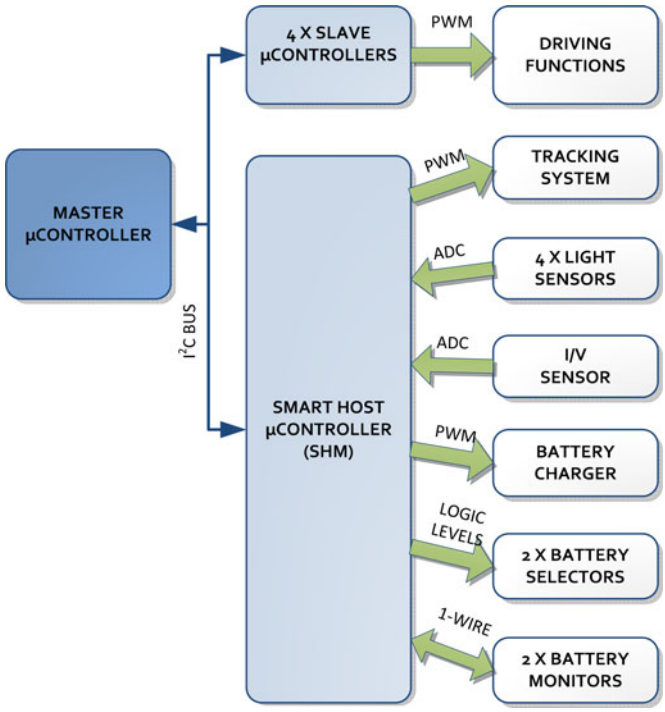

Fig. 2. Block diagram of the hardware architecture for VANTER.

A. Photovoltaic System With Solar Tracking Mechanism

When selecting the solar panels, VANTER physiognomy and consumption dictated its construction and electric requirements (see Section IV-C). The panel weight is a factor that limited its mechanical design; light-weight panels provide lower power consumption and require optimizing the robot's overall performance. The proposed PV system consists of three monocrystalline solar panels with laminated PET, whose dimensions are 200 mm × 250 mm × 3.2 mm and its weight is 0.7 kg per panel.

The PV system provides power, keeping in mind that voltages and currents generated must adapt to the maximum and minimum values of the hardware. However, since the environmental natural features cannot be predicted at each instant, the quantitative energy from solar radiation cannot be predicted either. Thus, one of the main proposals of this paper is the implementation of a solar tracking mechanism aimed at increasing power levels in the PV panels. Unlike other rovers that use navigation techniques to guide their panels toward the Sun [12], VANTER's mobility does not represent a disadvantage, since the proposed tracker system looks for the most powerful light source. Solar tracker prototypes built in mobile robots have proven that orientation of PV systems leads to increased energy efficiency relative to systems with fixed solar panels (20–50% per collector) [23]. This gain depends on several construction strategies of the solar tracker such as the type of axis movement (either single or dual), type of sensors on which is based(photoresistors or photoconductive cells), and the accuracy rendered by the number of sensor pairs [24]–[26]. On the contrary, parasitic load consumption associated to the proposed configuration (a mobile solar panel, two batteries, and electronics) compared to a simple system (a fixed panel, a battery, and electronics) is increased between 1.14% and 21.42%. The consumption increment varies mainly due to the operation of the solar tracking system, which is based on servos; thus, standard dc motors is proposed to reduce the consumption up to 8.57%.

Fig. 4 shows the mechanical solar tracking system. This comprises (a) a fixed solar panel mounted horizontally on VANTER and (b) two panels with symmetrical movements. The mechanical structure is mounted on (c) an aluminum chassis on which the electronics were mounted. On top of this platform (d) a methacrylate panel with (e) two side supports has been assembled. The solar panels are mounted on (f) pan and tilt units formed by two DYS0213MGs metal gear servos. Each pair of digital servomotors allow soft rotations with an amplitude of 180° in (g) azimuth and (h) elevation, so that the solar panels can be oriented toward any part of the space.

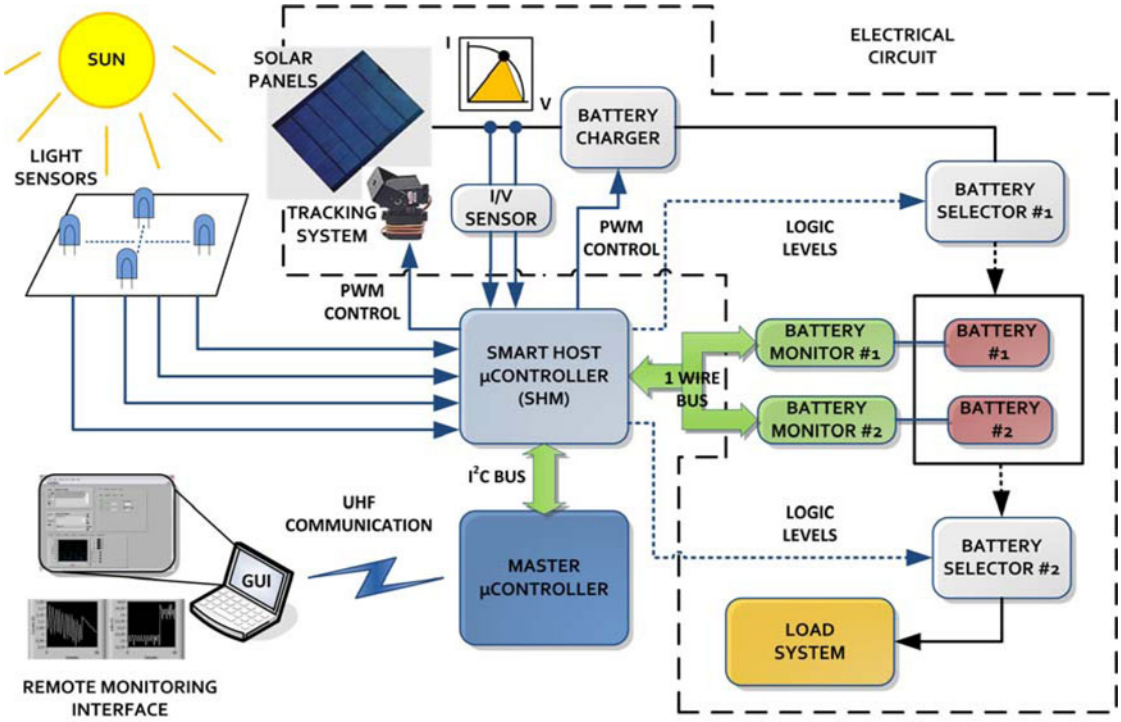

Fig. 3. Overall scheme of the power management system of VANTER.

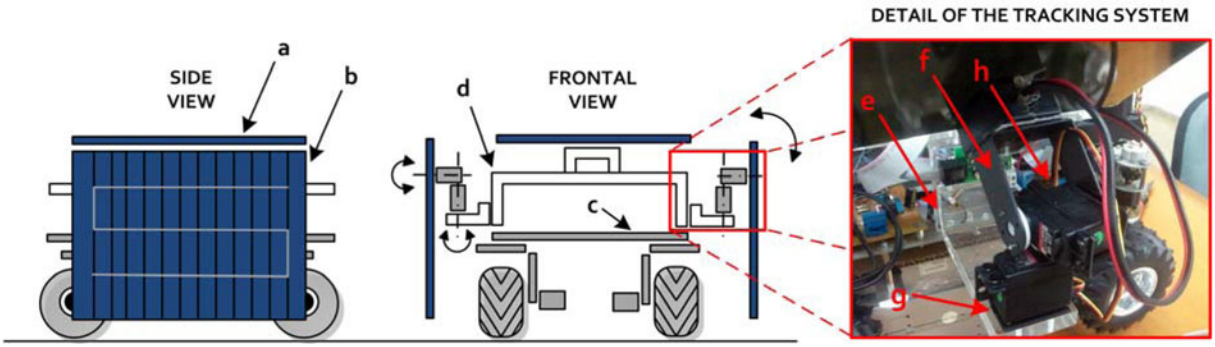

Fig. 4. Mechanical design of the solar tracking system of VANTER: (a) upper solar panel, (b) mobile solar panels, (c) aluminum chassis, (d) methacrylate chassis, (e) methacrylate support, (f) pan and tilt unit, (g) pitch servomotor, and (h) yaw servomotor.

The tracking system design is based on solar-type CdS photoconductive cells. This consists of four Hamamatsu S9648-100 photosensors mounted on a PCB attached to one solar panel of VANTER (see Fig. 5). The advantage of the selected devices is that they have a spectral sensitivity peak near 600 nm where light is considered to have more energy. To improve the performance of the tracking system, the photoconductive cells are arranged in a crosspiece and their field of vision is narrowed by means of opaque plastic tubes with an outwardly directed gap. Thus, this system provides a method to determine the brightness value at each cardinal point regarding the plane of the solar panel. The advantage over other systems based on solar mathematical equations is that this mechanism allows tracking as closely as possible to the solar position in any ambient light situation [23]. To this end, PCB allows calibrating photosensors' sensibility by means of variable resistors, which has the advantage of adapting to different brightness locations and lighting conditions.

Tracking the most powerful light source is possible because analog signals are obtained by the photosensors since they already include both amplifier and signal conditioner integrated circuits. Proportional light values are compared in pairs and, from their difference, adjusting the control signal for azimuth and elevation required by the tracking system. Each servo is controlled by a pulse width modulation (PWM), whose duty cycle determines the required rotation. Instead of increasing or decreasing the duty cycle at fixed values until servos face the light source, rotations are achieved by means of PWM signals generated as follows:

$$\mathbf{y} = \exp\left(\frac{x+30}{20}\right). \tag{1}$$

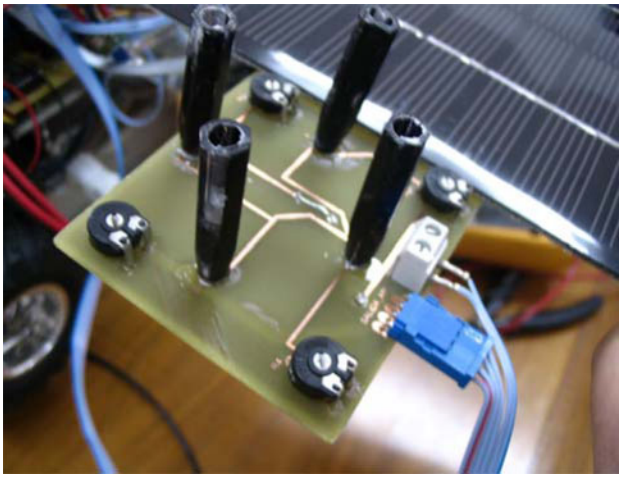

Fig. 5. Board of photosensors, light pipes with interference ribs and CdS cells inside the plastic cases.

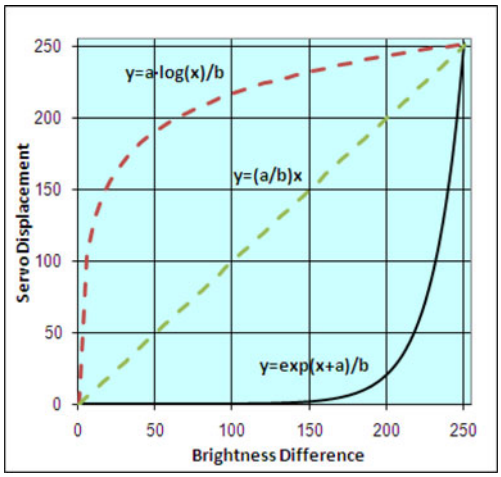

Fig. 6. Graphical representation of different servo control signals: equation implemented (continuous line) and other equations studied (dashed line).

This mathematical expression responds to an SHM-programmed algorithm where **y** stands for servo displacement, x is the difference of illumination between each couple of photosensors, and constants are values experimentally obtained in ground testing (see Fig. 6). The advantage of this strategy relative to other types of equations (i.e., linear or logarithmic) is the servos performing large displacements when the lighting values between each pair of photosensors evince high discrepancies on its axis. Similarly, shorter and accurate shifts are obtained when lighting values are approaching the most powerful light source. In this way, the pan and tilt units try to place mobile solar panels perpendicularly to the most intense light source available. Higher energy collection is therefore possible. On the other hand, the tracking algorithm also takes into account VANTER's kinematics configuration. Thus, it prevents servomotors from reaching limit positions during rotation so as to prevent solar panel from colliding with other robotic elements.

B. Batteries Switching System

The switching system consists of two MAX1538EVKIT selectors with break-before-make operation logic. Their function is connecting electrically the charge and discharge paths between the batteries, the charger module, and the load system (see Fig. 7). That is, selector 1 is inserted between the charger and the dual-battery pack. Its function is routing the current from the PV panels to the input of the charger and, from there, to the battery selected in each moment. Selector 2 is used to connect the selected battery to the load system. Therefore, the dynamic connections of the electric circuit are carried out according to the SHM-defined logical operation mode. This is based on the voltage thresholds programmed into the control algorithm (see Sections III-C and IV-B).

Table II shows an example of battery selector operation. In the first row, selector 1 was programmed to charge battery 1 while selector 2 is preset to discharge battery 2. Charge current obtained from the PV panels is routed to the charger through selector 1 and, from the charger, to the selected battery. Likewise, the discharge current of battery 2 is routed to the load system through selector 2. The main advantage of the dual selector system is that it allows hot swapping of separated power supplies. In addition, in case both batteries were fully discharged, a working mode was programmed in selector 1 to supply the load system directly from the PV panels.

C. Charging and Discharging System

When describing the implemented system, two different parts can be distinguished: a first one exclusively devoted to the intelligent management of the charging/discharging process, including controlling and monitoring sensor signals, and a logical part devoted to power flow management through VANTER energy sources.

MAX17005BEVKIT was the charger system used. This device consists of a dc–dc synchronous-rectified converter with step-down topology (efficiency over 90%) (see Fig. 8). The charger system is controlled by the SHM using a PWM signal applied to one of its terminals and supplies each battery according to a programmed algorithm. Between the PV system and the charger system there are a voltage conditioning capacitor and an *I*/*V* sensor from AttoPilot with 0–3.3 V output. The capacitor C_1 prevents voltage at the charger input pin V_{ch} from falling below the charge voltage of the battery cells V_{cv} when solar power is not capable of providing appropriate voltage level V_s. During that instant the capacitor is discharged with a current I_{ch} through the dc–dc converter. The role of the *I*/*V* sensor is detecting the current and voltage levels that solar panels provide to the charger device.

The algorithm implemented in the SHM consists of a charge regulation by increasing the output current of the charger module according to the MPP. The MPP-tracking scheme is based on the dynamic power path management (DPPM) function described by Texas Instruments Incorporated [27]. This low-cost solution is a simplified MPP tracker able to harness 90–95% of maximum power. On this basis, a voltage variation in the PV panels is detected by the *I*/*V* sensor as a power variation

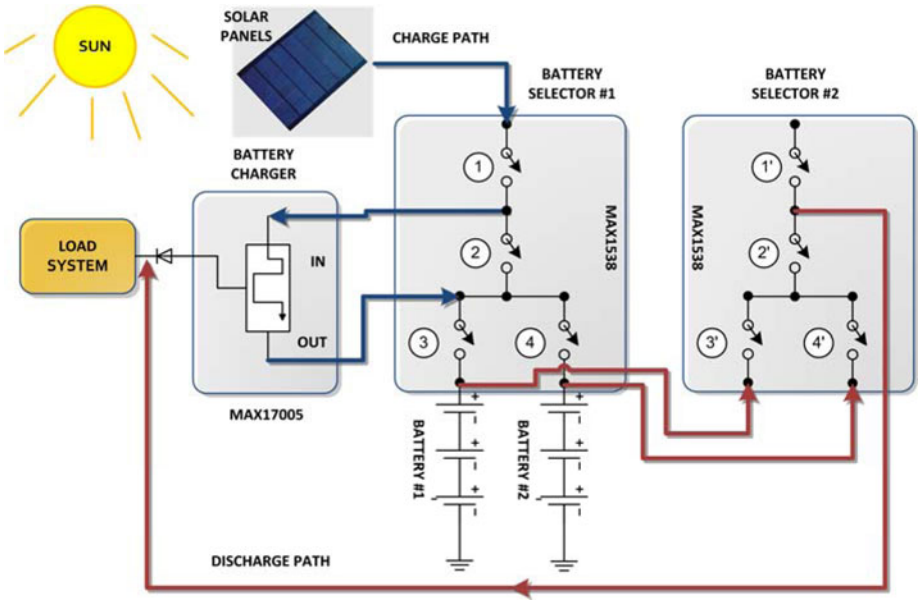

Fig. 7. Overall connection diagram for batteries selectors. The logical operation for charging and discharging modes is shown in Table II.

(see Fig. 8). These signals are used by the SHM to enable, disable, and control the charge current of the charger by means of a PWM signal. If the algorithm detects that light conditions provide higher output power at the PV panel, the SHM increases the output current of the charger up to the maximum regulation current. If light conditions cause a power drop in the PV panels, the SHM staggeringly reduces the current drawn to the battery until power stabilizes at the PV panels. In case of reaching the maximum allowable voltage for battery charging, the SHM algorithm drops out generated power reducing the output current of the charger device. Subsequently, the SHM proceeds to search a new maximum efficiency point as described previously. Consequently, the solar panels were sized to obtain a voltage suitable for this operation; therefore, the MPP is set with a voltage higher than the cutoff level of the dc–dc converter. This allowed us to implement a protection scheme against drops in solar power input to improve system performance and reliability (see Section V).

TABLE II
LOGICAL OPERATION MODE OF THE BATTERY SELECTORS

Battery Selector	1	2	3	4	1'	2'	3'	4'
#1 Charging & #2 Discharging	C	O	C	O	X	C	O	C
#1 Discharging & #2 Charging	C	O	O	C	X	C	C	O

C = Closed, O = Open, X = No Connected

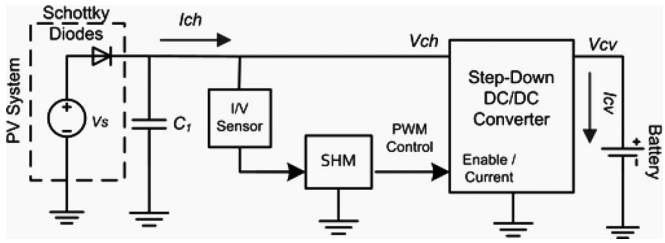

Fig. 8. Connection diagram of the charger system.

D. Batteries Monitoring System

The aim of the monitoring system is maximizing the life and energy storage of Li–Po cells. Therefore, the main function of this system is monitoring the state of charge (SoC) of the batteries and accurate control of the charging–discharging cycles. The use of a dual battery monitor system was required for control and parameter measurement. This module consists of two DS2788EVKIT+ integrated circuits manufactured by Maxim-IC. Each of these is connected to the batteries in parallel—so that the charge/discharge current passes through its measuring resistor—and by means of a 1-Wire bus multidrop type, both to the load system and the charger through the SHM. The main advantage of the dual monitoring system is that it allows continuous measurement of both the capacity of the battery in charge as well as of the one being discharged. Among other essential monitored parameters such as voltage, current, and temperature—which prevent batteries from working near their warming limits—the monitor displays some other important parameters such as the batteries' SoC, relative capacity (%), absolute capacity (mAh), state of health (SoH), and internal resistor (R_{int}).

E. Rechargeable Battery System

The design implemented in this paper proposes the use of two separate battery units working alternately [see Fig. 9(a)]. Thus, one of the batteries receives the charge current from the PV system while the other provides VANTER with all the energy it requires. Unlike other designs, in a conventional system the power source is used to recharge a single battery [see Fig. 9(b)]. As a disadvantage, the robot can only be used when the battery is fully charged and must remain idle during the recharging

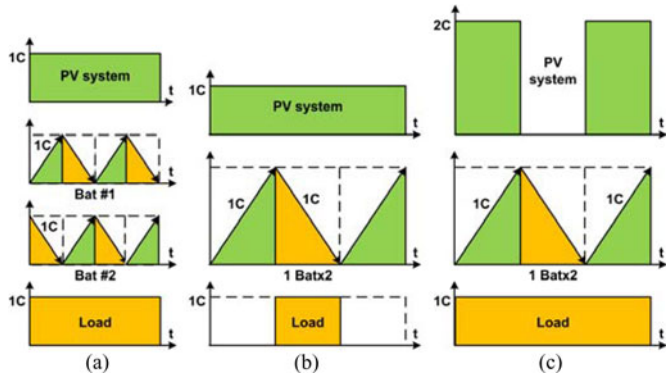

Fig. 9. Different strategies of solar-powered robots with battery system: (a) dual battery system, (b) conventional system, and (c) load sharing system.

process. On the contrary, in load sharing systems whose delivered solar energy is shared with the load while the battery is charging, power requirements at the source are higher [see Fig. 9(c)]. This means larger surface and therefore heavier solar panels. However, space and weight are critical design requirements in many small robotic vehicles. The implemented design in this paper proposes independent charging and discharging processes, thus dividing the problem into two batteries. A relatively good compromise between total weight, available capacity, and source-required power is reached. This strategy implies a smaller PV system to power a single smaller battery at a time and, therefore, solar panels are more economical. This goal was prioritized in this project. On the other hand, implementing a redundant system in which each battery is sized to cover VANTER's full consumption has the advantage that any power supply unit can easily be substituted in case of failure; this increases the system reliability. A typical system that sizes its consumption with a single battery delivering the required power at all times cannot dispense its supply unit.

The rechargeable system comprises two NanoPack V2 batteries of three Li–Po cells connected in a 3S2P configuration. The reasons for their choice were their high efficiency (98%), energy density (200 W·h/kg and 2300 W/kg), and long life (1400 cycles) in addition to their low size and weight without compromising a feasible cost. Thus, each battery provides the system with a capacity of 2400 mAh with a maximum voltage $V_{\rm oc} =$ 12.6 V and a size of $36 \times 35 \times 65$ mm^3.

F. Remote Monitoring Interface

In addition to the GUIs of the navigation system and the 5-DOF manipulator arm aboard VANTER—as described in [20]—the power management system presented in this paper may also be monitored from a remote PC (see Fig. 10). The virtual instrument is divided into several functional areas that facilitate the composition of the communication packets between the remote PC and VANTER by means of setup menus (a) and displays (b) and (c). The graphical representation of the values allows real-time verification of solar panel-generated voltage and current, batteries' current, voltage, and capacity as well as SoC and discharge, operation temperature, servo position, and photodiodes light level. As an example of the monitoring interface operation, the switching states of the batteries current (d) and voltage (e) during the charging and discharging processes are shown in different tabs. Finally, tab (f) displays both photosensor-generated voltage levels and the magnitude and angle of the resulting vector.

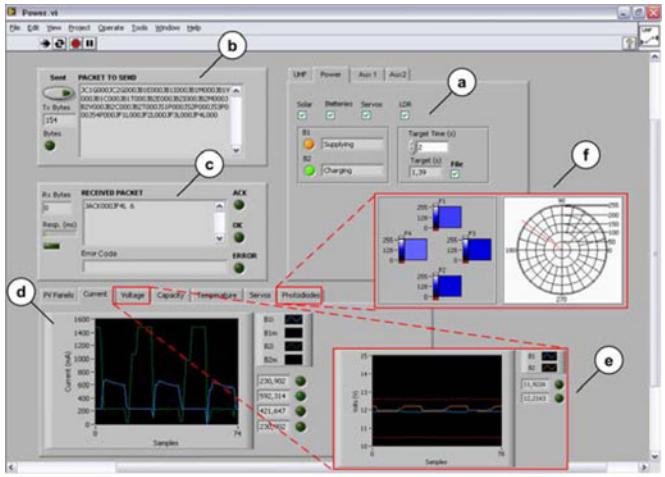

Fig. 10. GUI of the power management system: (a) setup, (b) and (c) UHF system, (d) PV panels, (e) batteries monitor, and (f) solar tracker system.

TABLE III
POWER DEMAND OF VANTER BASED ON THE RESULTS OBTAINED FROM GROUND TESTING

Operation Mode	Average Current
1 servomotor at idle position (5 V)	8 mA
1 servomotor moving (5 V)	150 mA
Only active electronics	250 mA
Active electronics & 4 wheels turning in flat terrain	1400 mA
All load operating & 4 wheels turning with steep slope	2000 mA

IV. POWER SYSTEM DESIGN

This section presents the sizing of the batteries system, the parameterization of the charging and discharging algorithm, and the sizing of the PV system in more detail.

A. Batteries Sizing

Each battery was sized taking into account both the maximum system consumption and VANTER continuous consumption under different operation conditions (see Table III). It should be also guaranteed that maximum system consumption is always below the maximum battery-deliverable discharge. Nevertheless, an Li–Po battery working at its maximum continuous discharge has the disadvantage of not providing the required performance and shortening its lifetime (e.g., 80% of capacity for 500 cycles at 10 C). Thus, keeping in mind that the selected batteries deliver peak currents of 23 C (over 55 A) and sustain a continuous consumption of 15 C (36 A), VANTER consumption requirement is fully covered. Thus, setting the required backup time, the capacity of each battery can be estimated by means of

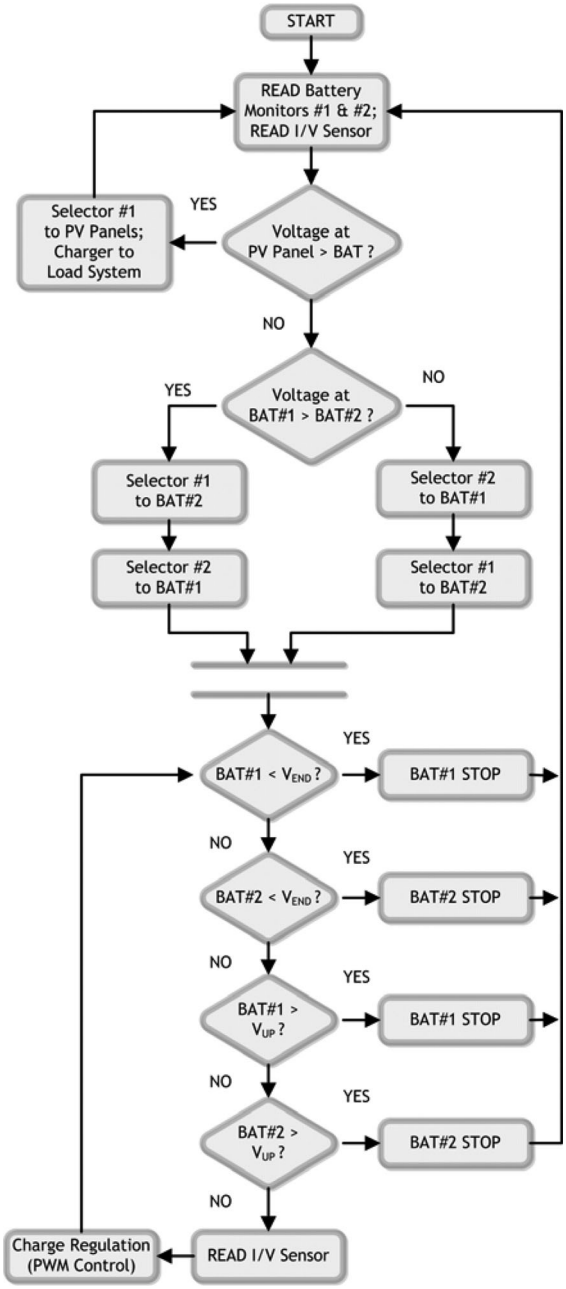

Fig. 11. Algorithm of the charging and discharging cycle.

the following formula:

$$\text{Capacity}\,(\text{mAh}) = \frac{t_{\text{on}}(\text{min}) \times \text{Current demand}\,(\text{mA})}{60\,\text{min/h}}. \quad (2)$$

Setting an operation time $t_{\text{on}} = 1$ h and a maximum consumption of 2000 mA—as expected in Table III—a capacity of 2000 mAh is then required. Considering a difference of ∼15% between the maximum and nominal capacity of a battery, a battery of 2400 mAh—as those chosen in this paper—covers this operation time.

TABLE IV
CAPACITY OF GENERATION OF EACH PV PANEL BASED ON THE RESULTS ACHIEVED FROM GROUND TESTING

Type of Light	V_{oc}	I_{sc}
UV ligh (100 W)	14.0 V	40 mA
Solar radiation	14.8 V	493 mA
Halogen light (1500 W)	15.2 V	400 mA
Halogen light (100 W)	15.2 V	340 mA

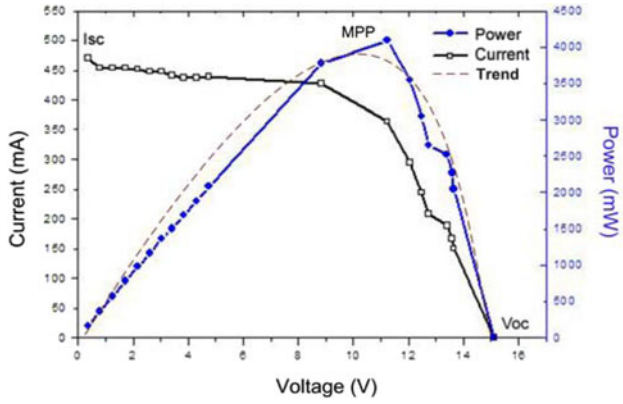

Fig. 12. *I–V* characteristic and output power of a solar panel at 23 °C and solar irradiance of 940 W/m^2.

B. Charge and Discharge Parameterization

On the other hand, threshold values for the dynamic charging/discharging regulation were defined in the SHM-programmed algorithm to prevent Li–Po batteries from damaging and to extend their life cycle (see Fig. 11). The charging and discharging process parameterization has been set considering the battery electrical model, where the battery stands for a voltage source with an internal resistor in series R_{int} specified by the manufacturer. Considering the voltage drop across the battery ($V_{\text{int}} = 0.3$ V) and a cutoff voltage V_{cutoff} for the charging and discharging algorithm, a maximum and minimum voltage V_{up} and V_{end} were defined for the charging and discharging protection conditions accordingly (see Section V).

C. Sizing of the Photovoltaic System

The power requirement of the PV system results from the estimation of the voltage and current values that the charger supplies to the battery (see Fig. 8). The maximum voltage at the charger output corresponds to the voltage of the fully charged battery during voltage regulation, which in this case corresponds to $V_{\text{oc}} = 12.6$ V. In a dc–dc converter with step-down topology a voltage higher than 12.6 V is required at the input, so the PV panel voltage at the MPP must exceed this value. Besides, each battery employs a capacity of 2400 mAh, its charge being advisable at a rate between 0.2 and 0.7 C. This corresponds to a charge current between 480 and 1680 mA, with an intermediate value of 0.5 C (1200 mA) a relatively good choice. Thereby, according to these considerations, the power required by the PV system is

$$P_s = P_{\text{schottky}} + (P_{\text{bat}}/\text{Efficiency}) \quad (3)$$

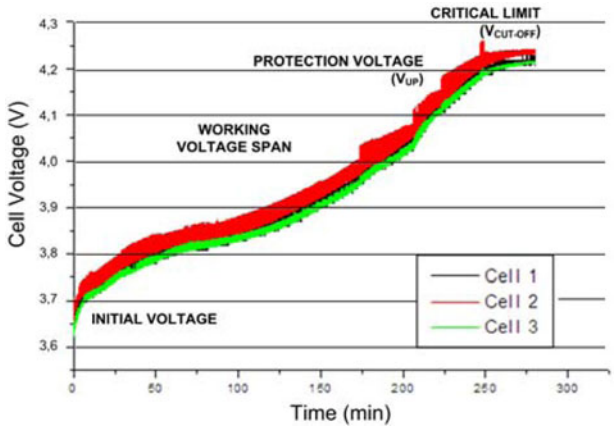

Fig. 13. Characteristic of the charge voltage measured in the cells battery.

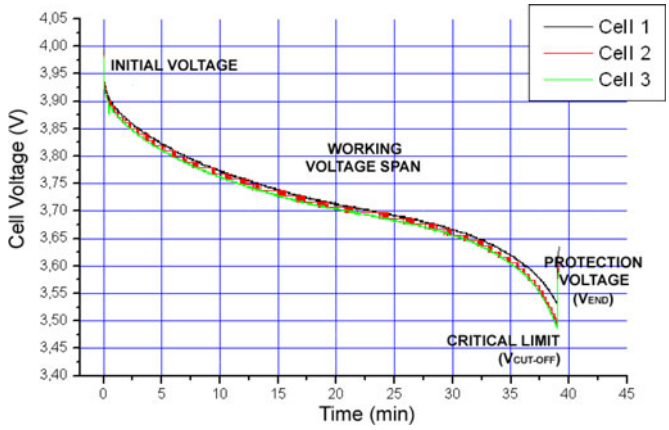

Fig. 14. Characteristic of the discharge voltage measured in the cells battery.

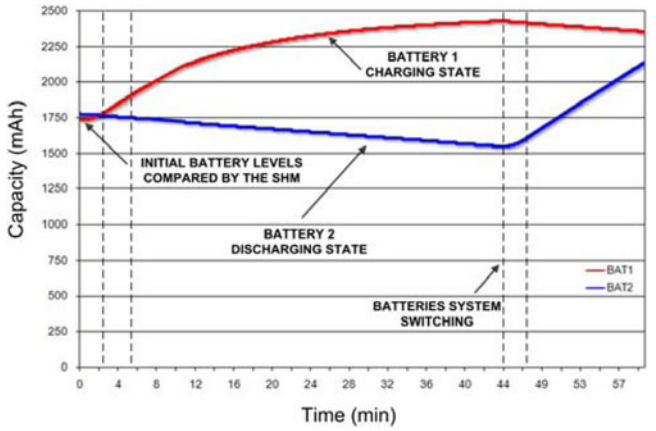

Fig. 15. Capacity curves in the batteries for a charging and discharging cycle.

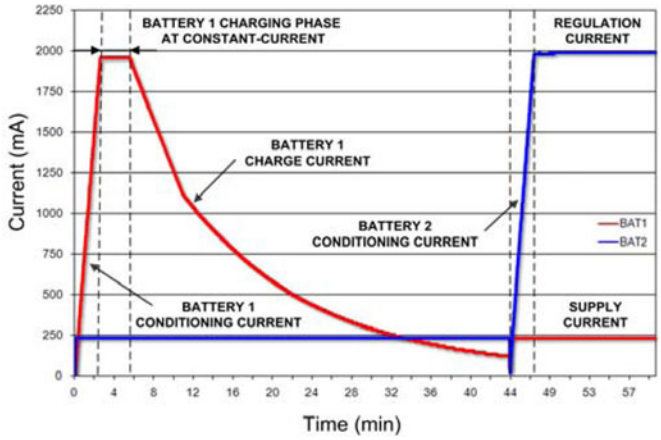

Fig. 16. Current curves in the batteries for a charging and discharging cycle.

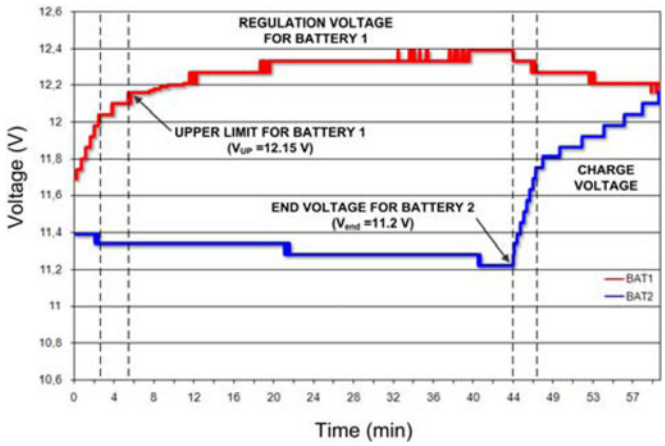

Fig. 17. Voltage curves in the batteries for a charging and discharging cycle.

where P_{schottky} is the power loss across the Schottky diodes that protect the PV panels, P_{bat} is the power delivered to the battery in the charging process considering 90% charger efficiency, according to the manufacturer. As a result, it is obtained that $P_s = 16.56$ W.

Assuming P_s tolerance is within 10%, power requirement is covered with a set of three PET panels as those chosen according to the manufacturing specification ($V_{\text{MPP}} = 14$ V, $I_{\text{MPP}} = 430$ mA, and $P_{\max} = 6$ W). In short, it complies that $P_{\max} \cdot n > (P_s \pm 0.1\ P_s)$, where n stands for the three solar panels electrically connected in parallel to comprise the PV system.

V. Experimentation

Different tests with the three solar panels were completed to assess power generation under different lightning conditions (see Table IV). The *I–V* characteristic of the solar panels was obtained by using a decade box consisting on a set of variable test resistors. Thus, Fig. 12 shows the output power versus current and voltage of a PV panel where the MPP is achieved at 23∞C with solar irradiance of 940 W/m^2.

On the other hand, an example of the experimentation carried out with a battery is shown in Fig. 13. The graph shows the charge curve of three Li–Po cells at a rate of 0.2 C (0.5 A) and $V_s = 12.25$ V. Measurements were taken in each battery cell at periods of 100 ms using a National Instruments USB-6009 DAQ. The figure shows the different regulation states from the initial voltage to the protection voltage V_{up}, above which a portion of unused voltage is defined V_{cutoff} to avoid irreparable

damages in the Li–Po batteries and thus favor greater safety. Fig. 14 shows the discharge curve of the Li–Po cells obtained at a rate of 1 C (2.4 A) through an external test resistor $R_L = 4.7\,\Omega$. As shown, discharge voltage varies from the initial voltage to the protection voltage $V_{\rm end}$, below which a portion of unused voltage is defined likewise $V_{\rm cutoff}$.

As an example of the battery system working in an alternate way, Figs. 15–17 represent the charging and discharging operation proposed in this paper. The capacity stored and delivered to the load system in terms of power during the charging and discharging states is shown in Fig. 15. Initially, the algorithm of the SHM detects the battery with lower capacity and carries out its charging while the battery with higher capacity supplies the load system. Thus, in the first tract of Fig. 16 battery 1 receives the charge current until reaching a set rate of $\sim$2 A, while battery 2 is only supplying VANTER active electronics ($I_L \sim$250 mA). The graph illustrates how battery 1 passes from the constant-current charging phase to the constant-voltage charging phase when $V_{\rm up}$ reaches 12.15 V for this test (see Fig. 17). Then, the charge current of battery 1 begins to drop while stabilizing the voltage and battery 2 continues in discharge until the end voltage is reached ($V_{\rm end} = 11.2$ V for this test). In this point, at $t = 44$ min the switching of the batteries system is observed. The turn-OFF and turn-ON times of the batteries take place in a time $t_{\rm trans} = 6\ \mu$s in which no supplies are connected to each other during the transition. In summary, the constant-current charging phase—in which the Li–Po battery is considered charged to a 75–80%—takes up relatively short time, while the following phase (80% to 95–100%) takes much longer as shown.

VI. Conclusion

This paper has presented a smart energy management system applied to a robotic platform called VANTER, an autonomous unmanned vehicle devoted to exploration tasks. The proposal includes the construction of a solar tracker mechanism based on mobile PV panels aimed at increasing system energy. Its main advantage is that the amount of generated power is independent from the rover's mobility, since the proposed mechanism is capable of tracking maximum light intensity.

Delivering the systems' energy requirements while recharging the backup battery was made possible by implementing a dual system of selectors, monitors, and batteries. This strategy implies small solar panels to power a single battery at a time. A relatively good compromise between total weight, capacity available, and source-required power is reached. This solution does not attempt to achieve high charging times or great operating times but to prove a sustainable and commercially feasible solution applied to a robotic vehicle. In this sense, an SHM was designed for optimal charge regulation by means of an MPP-tracking scheme based on the DPPM.

Experimentation shows that the charging and discharging processes that require careful Li–Po cells became possible due to a fine SHM-implemented control algorithm. To this end, a practical implementation of the switching battery system according to the operating limit values is shown.

References

[1] D. L. Shirley, "Mars pathfinder microrover flight experiment—A paradigm for very low-cost spacecraft," *Acta Astronaut.*, vol. 35, pp. 355–365, 1995.

[2] H. J. Eisen, L. C. Wen, G. Hickey, and D. F. Braun, "Sojourner mars rover thermal perfomance," presented at the 28th Int. Conf. on Environmental Systems, Danvers, MA, 1998.

[3] Stefano, B. V. Ratnakumar, M. C. Smart, G. Halpert, A. Kindler, H. Frank, S. Di, R. Ewell, and S. Surampudi, "Lithium batteries on 2003 mars exploration rover," presented at the IEEE 17th Annu. Battery Conf. Applications and Advances, Long Beach, CA, pp. 47–51, 2002.

[4] M. Bajracharya, M. W. Maimone, and D. Helmick, "Autonomy for mars rovers: Past, present, and future," *Computer*, vol. 41, no. 12, pp. 44–50, 2008.

[5] A. K. Baluch, "Re-use of exomars rover on icy moons of jupiter," M.Sc. thesis, Dept. Space Sci., Crandfield Univ., Swindon, U.K., 2010.

[6] The Rover Team, "The ExoMars rover and Pasteur payload Phase a study: An approach to experimental astrobiology," *Int. J. Astrobiol.*, vol. 5, no. 3, pp. 221–241, 2006.

[7] J. L. Bresina, M. G. Bualat, L. J. Edwards, R. J. Washington, and A. R. Wright, "K9 operation in May '00 dual-rover field experiment," presented at the 6th Int. Symp. Artificial Intelligence, Robotics and Automation in Space, Montreal, QC, Canada, 2001.

[8] P. S. Schenker, E. T. Baumgartner, P. G. Backes, H. Aghazarian, L. I. Dorsky, J. S. Norris, T. L. Huntsberger, Y. Cheng, A. Trebi-Ollennu, M. S. Garrett, B. A. Kennedy, and A. J. Ganino, "FIDO: A field integrated design & operations rover for mars surface exploration," presented at the 6th Int. Symp. Artificial Intelligence, Robotics and Automation in Space, Quebec, QC, Canada, 2001.

[9] T. Kubota, Y. Kunii, Y. Kuroda, and M. Otsuki, "Japanese rover test-bed for lunar exploration," in *Proc. Int. Symp. Artif. Intell., Robot. Automat. Space*, no.77, 2008.

[10] M. S. Schneider, A. Bertrand, R. Lamon, P. Siegwart, R. van Winnendael, and A. Schiele, "SOLERO: Solar powered exploration rover," presented at the 7th ESA Workshop Advanced Space Technologies for Robotics and Automation, Noordwijk, The Netherlands, 2002.

[11] P. Lamon, "The solero rover. 3D-position tracking & control for all-terrain robots," *Adv. Robot.*, vol. 43, pp. 7–19, 2008.

[12] B. Shamah, M. D. Wagner, S. Moorehead, J. Teza, D. Wettergreen, and W. L. Whittaker, "Steering and control of a passively articulated robot," presented at the SPIE Sensor Fusion and Decentralized Control in Robotic Systems IV, Oct. 2001.

[13] D. Wettergreen, N. Cabrol, V. Baskaran, F. Calderon, S. Heys, D. Jonak, A. Lüders, D. Pane, T. Smith, J. Teza, P. Tompkins, D. Villa, C. Williams, and M. Wagner, "Second experiment in the robotic investigation of life in the Atacama Desert of Chile," presented at the 8th Int. Symp. Artificial Intelligence, Robotics and Automation in Space, Munich, Germany, 2005.

[14] I. Nourbakhsh, E. Hamner, D. Bernsteinb, K. Crowleyb, E. Ayooba, M. Lotterc, S. Shellyc, T. Hsiud, E. Portera, B. Dunlaveya, and D. Clancye, "The personal exploration rover: Educational assessment of a robotic exhibit for informal learning venues," *Int. J. Eng. Educ.*, vol. 22, no. 4, pp. 777–791, 2006.

[15] J. H. Lever, L. R. Ray, A. Streeter, and A. Price, "Solar power for an antarctic rover," *Hydrol. Process*, vol. 20, pp. 629–644, 2006.

[16] L. E. Ray, J. H. Lever, A. D. Streeter, and A. D. Price, "Design and power management of a solar-powered cool robot for polar instrument networks," *J. Field Robot.*, vol. 24, no. 7, pp. 581–599, 2007.

[17] Y. Takahashi, S. Matsuo, and K. Kawakami, "Hybrid robotic weelchair with photovoltaic solar cell and fuel cell," in *Proc. Int. Conf. Control, Autom. Syst.*, Seoul, Korea, 2008, pp. 1636–1640.

[18] A. N. Wilhelm, B. W. Surgenor, and J. G. Pharoah, "Design and Evaluation of a micro-fuel-cell-based power system for a mobile robot," *IEEE/ASME Trans. Mechatronics*, vol. 11, no. 4, pp. 471–476, Aug. 2006.

[19] I. A. Anderson, I. A. Ieropoulos, T. McKay, B. O'Brien, and C. Melhuish, "Power for robotic artificial muscles," *IEEE/ASME Trans. Mechatronics*, vol. 16, no. 1, pp. 107–111, Feb. 2011.

[20] T. de Jesus Mateo Sanguino, "Contributions to the development of virtual and remote laboratories in robotics," Ph.D. dissertation, Dept. Electron. Eng., Comput. Syst. Automat., Univ. Huelva, Huelva, Spain, 2010.

[21] J. M. Andújar Márquez, T. de Jesus Mateo Sanguino, F. J. Aguilar Nieto, J. J. Chica Barrera, and M. J. Mola Mateos, "An image acquiring, processing and transfer system over bluetooth for an educational robotic platform," presented at the 7th Conf. Mobile Robots Competitions, Albufeira, Portugal, 2007.

[22] J. E. González Ramos, "Battery charging optimization with steerable solar cells," M.S. thesis, Dept. Electron. Eng., Comput. Syst. Autom., Universidad de Huelva, Huelva, Spain, 2010.
[23] A. B. Afarulrazi, W. M. Utomo, K. L. Liew, and M. Zafari, "Solar tracker robot using microcontroller," in *Proc. Int. Conf. Bus., Eng. Ind. Appl.*, 2011, pp. 47–50.
[24] S. Abdallah and S. Nijmeh, "Two-axis sun tracking with PLC control," *Energy Convers. Manage.*, vol. 45, pp. 1931–1939, 2004.
[25] C. Y. Lee, P. C. Chou, C. M. Chiang, and C. F. Lin, "Sun tracking systems: A review," *Sensors*, vol. 9, pp. 3875–3890, 2009.
[26] T. Jinayim, S. Arunrungrasmi, T. Tanitteerapan, and N. Mungkung, "Highly efficient low power consumption tracking solar cells for white-LED based lighting system," *World Acad. Sci., Eng. Technol.*, vol. 28, pp. 291–296, 2007.
[27] N. Smith, "Dynamic power path management simplifies battery charging from solar panels," Texas Instruments, Dallas, TX, Tech. Rep. SLUA394, 2006.

Tomás de Jesus Mateo Sanguino received the Ph.D. degree in electronic engineering from the University of Huelva, Spain, in 2010.

Currently, he is an Electronic Engineer and a Master in University Teaching. From 1998 to 2004, he had a scholarship at the National Institute of Aerospace Technology (INTA), Huelva, Spain, and was a Hired Engineer at the Spanish National Research Council (CSIC), Granada, Spain. Since 2004, he has been a Full-Time Associate Teacher in the Department of Electronic Engineering, Computer Systems and Automatics at the University of Huelva, Huelva, Spain. He has taken part as a researcher in 19 projects and has authored or coauthored more than 50 publications in various journals and conference proceedings, among which he has 12 papers in the SCI. His current research interests include robotics and mechatronics.

Justo E. González Ramos received the Industrial Engineering degree from the University of Huelva, Huelva, Spain, in early 2010 and it is a specialized Bachelor's in Industrial Electronics.

He has worked since 2009 as a hired engineer at Abengoa SOLAR, Seville, Spain, and his research interests are focused on robotics and photovoltaic systems.